Wildlife exposure to SARS-CoV-2 across a human use gradient

Amanda R. Goldberg[1]*, Kate E. Langwig[1], Jeffrey Marano[2,3], Pallavi Rai[2], Amanda K. Sharp[4], Katherine L. Brown[5,6], Alessandro Ceci[7], Macy J. Kailing[1], Russell Briggs[7], Clinton Roby[7], Anne M. Brown[5,8,9,10,11], James Weger-Lucarelli[2,6], Carla V. Finkielstein[1,5,6,10,11,12]†*, Joseph R. Hoyt[1]†

[1]*Department of Biological Sciences, Virginia Tech, Blacksburg, Virginia, USA*
[2]*Department of Biomedical Sciences and Pathobiology, Virginia Tech, Blacksburg, Virginia, USA*
[3]*Translational Biology, Medicine, and Health Graduate Program, Virginia Tech, Roanoke, VA, USA*
[4]*Program in Genetics, Bioinformatics, and Computational Biology, Virginia Tech, Blacksburg, VA, USA*
[5]*Virginia Tech Carilion School of Medicine, Virginia Tech, Roanoke, VA, USA*
[6]*Center for Emerging, Zoonotic, and Arthropod-borne Pathogens, Virginia Tech, Blacksburg, VA, USA*
[7]*Molecular Diagnostics Laboratory, Fralin Biomedical Research Institute, Virginia Tech, Roanoke, VA, USA*
[8]*Department of Biochemistry, Virginia Tech, Blacksburg VA, USA*
[9]*Data Services, University Libraries, Virginia Tech, Blacksburg, VA, USA*
[10]*Virginia Tech Center for Drug Discovery, Virginia Tech, Blacksburg, VA, USA*
[11]*Academy of Integrated Science, Virginia Tech, Blacksburg, VA, USA*
[12]*Integrated Cellular Responses Laboratory, Fralin Biomedical Research Institute at VTC, Roanoke, VA, USA*

Amanda R. Goldberg, goldberg.amandar@gmail.com; Carla V. Finkielstein, finkielc@vt.edu

†Authors contributed equally

Author Contributions: A.R.G., K.E.L., and J.R.H. designed field research; A.R.G., M.J.K, and K.E.L performed field research; J.M., P.R. K.E.L., J.W, C.R, A.C., R.B., C.V.F., and J.R.H. contributed to field data analysis; A.K.S., A.B., K.B., and C.V.F contributed to molecular analysis; K.E.L., J.W., C.V.F., and J.R.H. provided project administration; Members of the Molecular Diagnostics Laboratory provided technical support; and all authors aided in interpreting results and to writing the paper.

Keywords: Omicron variant, cross-species transmission, spillover, SARS-CoV-2, wildlife

Abstract

The spillover of SARS-CoV-2 into humans has caused one of the most devastating pandemics in recorded history. Human-animal interactions have led to transmission events of SARS-CoV-2 from humans to wild and captive animals. However, many questions remain about how extensive SARS-CoV-2 exposure is in wildlife, the factors that influence wildlife transmission risk, and whether sylvatic cycles can generate novel variants with increased infectivity and virulence. We sampled 22 different wildlife species in Virginia, U.S.A. We detected widespread exposure to SARS-CoV-2 across six wildlife species. Using quantitative reverse transcription polymerase chain reaction, we detected SARS-CoV-2 RNA in the Virginia opossum and had equivocal detections in six additional species. Furthermore, we used whole genome sequencing to confirm the presence of SARS-CoV-2 and compare mutations present to known circulating strains. Species that exhibit peridomestic tendencies had high seroprevalence, ranging between 62%-71%, and sites with high human presence had three times higher seroprevalence than low human-use areas across all species combined. SARS-CoV-2 genomic data from an opossum and molecular modeling exposed one previously uncharacterized change to an amino acid residue in the Spike receptor binding domain (RBD), which predicts improved binding between the Spike protein and human angiotensin-converting enzyme (ACE2) compared to the dominant variant circulating at the time of collection. Overall, our results highlight widespread exposure to SARS-CoV-2 in wildlife and suggest that areas with high human activity may serve as important points of contact for cross-species transmission. Furthermore, this work highlights the potential role of wildlife as reservoirs for SARS-CoV-2.

Significance Statement

The emergence of SARS-CoV-2 has resulted in unprecedented consequences for humans across the globe. Transmission of SARS-CoV-2 among species has the potential to generate new and more virulent variants, posing a threat to both public health and animal populations. However, the ability of SARS-CoV-2 to infect wildlife other than white tailed deer and mustelids in nature remains unknown. We examined exposure to SARS-CoV-2 in 22 wildlife species, which are commonly found across the Eastern U.S. We found widespread SARS-CoV-2 exposure in six common wildlife species, which was elevated in areas with high human activity. Our results highlight the capacity of SARS-CoV-2 to spread through wildlife communities.

Main Text

Introduction

Severe acute respiratory syndrome coronavirus 2 (SARS-CoV-2), the causative agent of coronavirus disease 2019 (COVID-19), has resulted in over 600 million human cases and over 6 million deaths worldwide (1). As this pathogen becomes endemic in the human population, one of the greatest threats to public health is the resurgence of more transmissible and virulent SARS-CoV-2 variants. The considerable pathogen pressure imposed by the pandemic has caused concern around whether SARS-CoV-2 will spill into wildlife populations and establish a sylvatic cycle. Establishment of SARS-CoV-2 infections in a new host could result in novel mutations that increase virulence, transmissibility, or confer immune escape, which could negatively impact both human and wildlife populations.

Transmission to captive animals has been well documented (2-4), but SARS-CoV-2 detections in free-ranging wildlife are currently limited to only a few species including: the white-tailed deer (*Odocoileus virginianus*; (5-7)), and mustelids (8) such as the feral mink (*Neovison vison*; (9)) and the Eurasian river otter (*Lutra lutra*; (10)). Experimental infections and modeling of the functional receptor for SARS-CoV-2 (angiotensin-converting enzyme 2: ACE2) have shown that numerous wildlife species may be competent hosts (11-16). However, which wildlife species are infected in natural settings, where exposure to SARS-CoV-2 is likely to be indirect and at a lower exposure dose than in laboratory settings, remains unexplored.

Since the early detection of SARS-CoV-2 in 2019, numerous variants have been detected in humans and animals. Some variants that have become dominant in human populations have shown mutations that increase their infectivity (17). Questions remain about how these mutations will also impact the ability of the virus to infect wildlife. White-tailed deer samples have included lineages found in human samples, likely caused by transmission between humans and the deer (5), as well as unique mutations suggestive of deer to deer transmission (18). Human peridomestic species, such as deer, skunks, rats, and mice have all been found to be generally susceptible to the virus in laboratory settings (12). However, the implications of this for transmission to humans is unknown beyond the suggestion that minimal adaptation may be needed for transmission to occur within mink and deer following initial transmission from human to animals (19).

With increased numbers of susceptible and exposed host species, there is an increased risk of mutations that could lead to more virulent strains both within wildlife populations and humans. Studies have shown that SARS-CoV-2 is capable of producing large numbers of mutations, many appear neutral but some are associated with increased transmission rates and virulence (20). Furthermore, as SARS-CoV-2 adapts to not only human hosts, but potentially a wide diversity of wildlife hosts, there may be increased opportunities for mutations that could have

higher infectivity in both humans and wildlife. This could pose a problem for human health due to vaccine development aimed at human specific strains. If wildlife infected with novel strains of SARS-CoV-2 are able to transmit this virus back into human hosts and humans are still susceptible, new dominant strains may emerge, making vaccine failure more likely.

In order to examine how widespread SARS-CoV-2 exposure has been in wildlife communities, we collected nasopharyngeal and serum samples from 22 species in Virginia, U.S.A. We used a combination of quantitative reverse transcription polymerase chain reaction (RT-qPCR) and whole genome sequencing as well as neutralizing antibody surveys to examine wildlife exposure to SARS-CoV-2. We also examined the effects of urbanization and human use on seropositivity in animals.

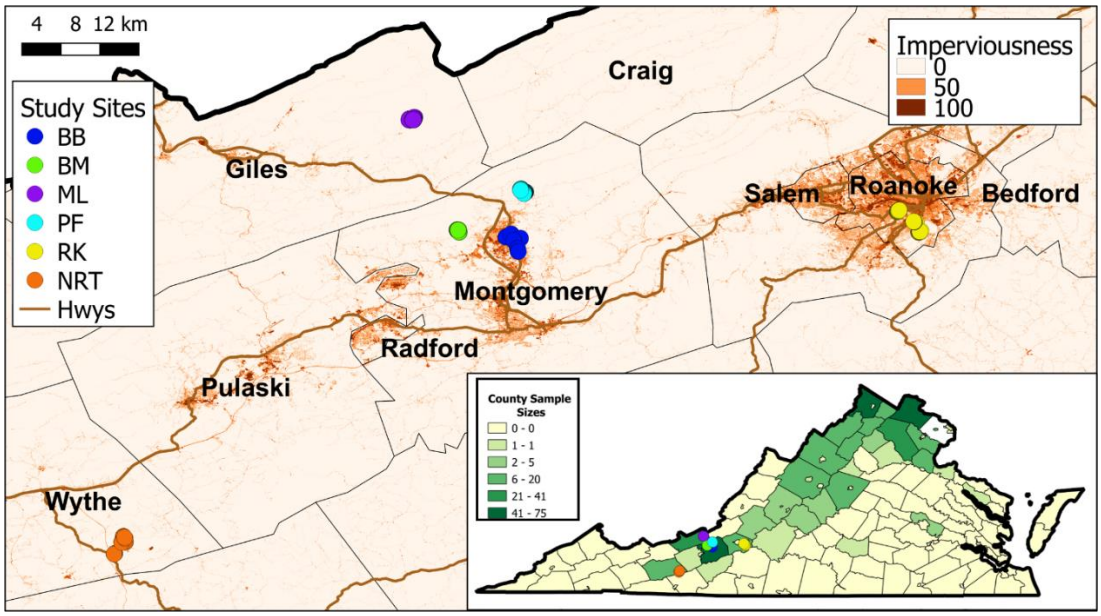

Figure 1. Location of the six study sites and counties where viral swabs were collected (larger panel). Orange shading represents imperviousness with darker shades of orange representing more urban areas. Serology samples were collected at all of the study sites except "PF". The inset panel represents all the counties where nasopharyngeal swabs were collected (from both wildlife rehabilitation centers and the 6 study sites). Darker green counties represent larger sample sizes. Each of the colored circles represents different trap locations and the colors indicates study site where we collected samples from live individuals within four counties in Virginia. Highways is abbreviated as Hwys. Study sites include: Blacksburg (BB), Brush Mountain (BM), Mountain Lake Biological Research Station (ML), Preston Forest (PF), Roanoke (RK), and New River Trails State Park (NRT); see supplemental methods for further site descriptions.

Results

We analyzed 418 samples (415 individuals) from 22 species collected across 35 counties in Virginia, U.S.A. (Table S1, Fig. 1). We conducted more detailed sampling across 10 species (111 samples; Table S1) from six sites across an urbanization gradient in Southwestern Virginia, where both nasopharyngeal swabs and serum samples were examined (Fig. 1).

We amplified RNA from two SARS-CoV-2 genes from a single Virginia opossum (*D. virginiana*; 1.3%, N=80; Fig. 2A, Table S2). Overall PCR prevalence based on just a single gene (*S* or *N*) amplification was ~5% with equivocal detections in 6 additional species. Red fox (*Vulpes vulpes*; 11.1%, N=9), Virginia opossum (10.0%, N=79), and white-tailed deer (*Odocoileus virginianus;* 10.0%, N=10) had the highest prevalence. Other species with a single gene amplification included the Eastern gray squirrel (*Sciurus carolinensis;* 3.5%, N=86), Eastern cottontail rabbit (*Sylvilagus floridanus*; 6.7%, N=75), raccoon (*Procyon lotor*; 2.2%, N=46), and bobcat (*Lynx rufus;* 50.0%, N=2).

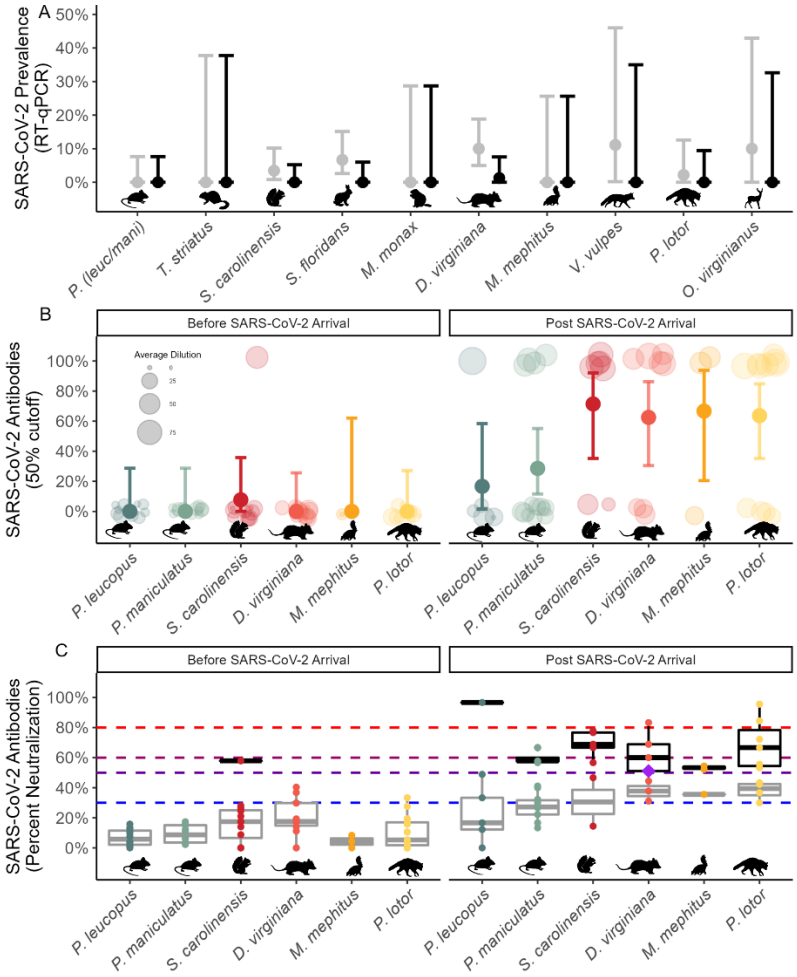

Figure 2. Results of SARS-CoV-2 exposure from nasopharyngeal and/or oropharyngeal swabs and serology data. Prevalence of (A) RT-qPCR detections (B) seroprevalence for species sampled both prior to SARS-CoV-2 arrival in 2020 and samples collected in our study from 2022 and 2023 and (C) percent neutralization of serum samples to SARS-CoV-2 sampled both prior and post SARS-CoV-2 arrival. Detections for RT-qPCR include species with >5 individuals sampled and both panels include the prevalence and 95% confidence intervals. Black points in panel (A) represent prevalence based on amplification of two of the three genes (N, S, and E) while estimates in gray include samples that amplified on a single gene. All samples had a Cq value <40. The size of each point in panel (B) is in relation to the

percent neutralization. Samples with a 50% or greater percent neutralization were considered positive samples. Error bars represent 95% confidence intervals. The top horizontal line (red) represents an 80% neutralization cut-off, followed by 60%, 50%, and 30% (blue) (C). The purple diamond represents a resampled Virginia opossum who was found conclusively RT-qPCR positive one month prior. Grey boxes represent median and interquartile range of samples with less than a 50% neutralization value. Black boxes represent the median and interquartile range of samples with greater than a 50% neutralization value. See Tables S2 and S3 for RT-qPCR Cq values <40 and percent neutralization values for all samples tested.

At the 50% neutralization cutoff, SARS-CoV-2 antibodies were detected in all six species where serum was collected, including the Virginia opossum (62.5%, N=8), striped skunk (*Mephitis mephitis*; 66.7%, N=3), raccoon (*Procyon lotor*; 63.6%, N=11), Eastern grey squirrel (71.4%, N=7), white-footed mouse (*Peromyscus leucopus;* 16.7%, N=6) and the deer mouse (*Peromyscus maniculatus*; 28.6%, N=14; Fig. 2B, Table S3). Percent neutralization from samples prior to the arrival of SARS-CoV-2 was significantly lower than those collected after SARS-CoV-2 arrival (t=-10.774, P < 0.001, Figure 2C). One sample from a squirrel sampled prior to the arrival of SARS-CoV-2 had percent neutralization of 58% (all other samples were substantially lower), and thus the probability of falsely detecting a positive given the 50% cutoff was 0.015 (N=67).

Furthermore, given our sample sizes paired with the high seroprevalence of wildlife post-SARS-CoV-2 emergence, the probability of detecting 0 positives in 5 species, and 1 positive in another species was very low (opossums: P<0.0001, skunks: P = 0.0370, white-footed mice: P = 0.1122, deer mice: P = 0.0176; raccoons: P<0.0001; squirrels: P<0.0001; Table S4). Four samples (two raccoons, one opossum, and one white-footed mouse) had a percent neutralization above a more conservative 80% cut-off, further supporting that SARS-CoV-2 exposure is likely in these species (Fig. 2C). The opossum with two-gene amplification and WGS, was trapped one month afterwards and serum samples collected revealed a percent neutralization value of 51.1%.

We found a positive relationship between urbanization (imperviousness) and wildlife seroprevalence at the 50% cutoff (intercept: -0.61 $\pm$ 0.38 SE, urbanization slope 0.04 $\pm$ 0.02 SE, P = 0.024, Fig. 3A). Antibody detections were highest (80%, N=5) at one of the least urban sites which is a highly utilized state park (average imperviousness 1.5%), and more closely matched seroprevalence at two of our urbanized sites (70%, N=10 and 67%, N=12). However, human visitation at this site and other urbanized sites were more than 20x higher compared to the low visitation sites (Table S5). We found a positive relationship between human presence and seroprevalence of SARS-CoV-2 (univariate linear mixed model with species as a random effect; intercept: -0.039 $\pm$ 0.31 SE, human presence coeff: 0.764 $\pm$ 0.31 SE, P = 0.014; Fig 3B, Fig. S5). Additionally, we found a similar positive relationship between human residence and seroprevalence of SARS-CoV-2 (intercept: -0.039 $\pm$ 0.31 SE; Fig. S1, human presence coeff: 0.726 $\pm$ 0.31 SE, P = 0.019; Fig S2).

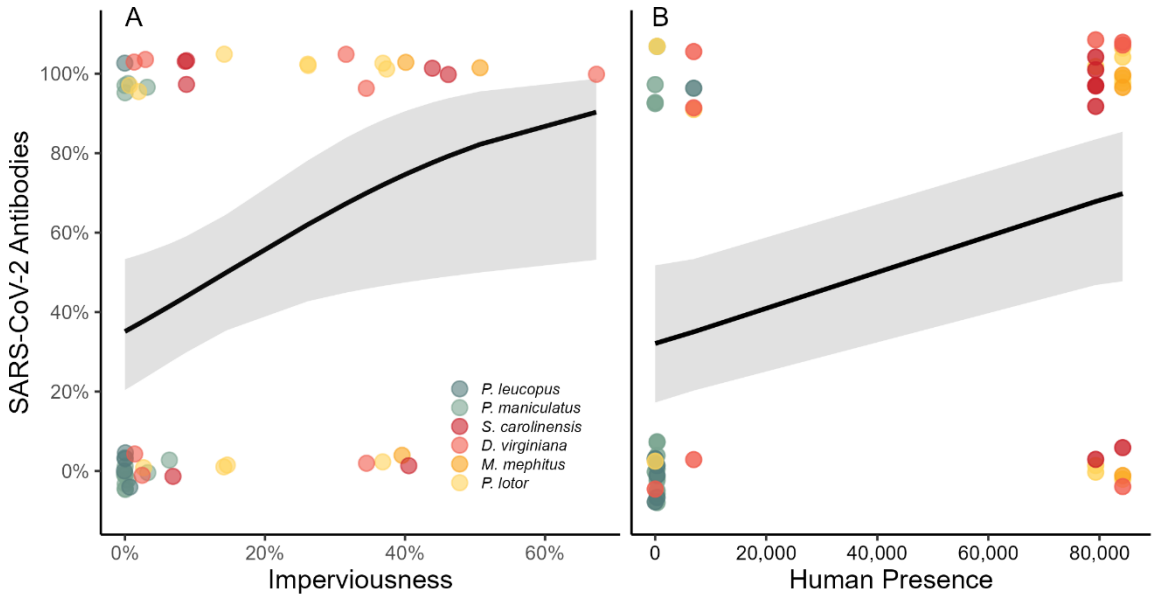

Figure 3. Examination of SARS-CoV-2 exposure across species and the human-wildlife interface. Panel (A) shows the relationship between urbanization (imperviousness) and seroprevalence collected from 5 different sites in VA, USA. Panel (B) shows the effects of monthly human presence (population density collected from the 2020 U.S. Census within the trapping area of each site (Blacksburg) or use estimates from trail counters or land-owners) on seroprevalence. Grey ribbons (shaded areas around the line) represent 95% confidence intervals.

We conducted WGS of the SARS-CoV-2 variant detected in the opossum which revealed several mutations shared within the Omicron clade as well as a unique amino acid substitution not previously identified in other human-infected SARS-CoV-2 virus at the time of collection (Table 1). The opossum sequence shared defining mutations in *ORF1a*/*b*, *S*, *E*, and *M* genes found in the BA.2 Omicron lineage (Fig. 4).

Table 1. Summary of mutations identified in the Virginia opossum (*Didelphis virginianus*)

SNP	Gene	Mutation
C7749T	*ORF1ab*/*NSP3*	Missense $T^{2495}I$
T16342C	*ORFab*/*Helicase*	Missense $S^{5390}P$
A20304G	*ORFab*/*EndoRNAse*	Synonymous
A22974T	*S*	[1]Missense $E^{471}V$
G23955A	*S*	[2]Missense $G^{798}D$

[1]Fig 5A, [2]Fig.5A, Fig. S3A, Fig. S4

At the time of the sample collection and genomic analysis, May 2022, we could not confidently assign a variant name. However, more recent phylogenetic analysis of the whole genome showed the isolate clustered within the NextStrain clade 21L (BA.2; Omicron) and assigned the PANGO lineage BA.2.10.1, also named BJ.1, using UShER (Fig. 4). This Omicron sub-linage includes the $G^{798}D$ mutation found in the Spike protein. The nearest neighbor (EPI_ISL_14334179), which was detected in New York state after our sampling, contains all the nucleotide and amino acid mismatches as the opossum sequence as compared to the reference sequence from Wuhan, China, except for A22974T ($E^{471}V$) which appears to be unique to the opossum.

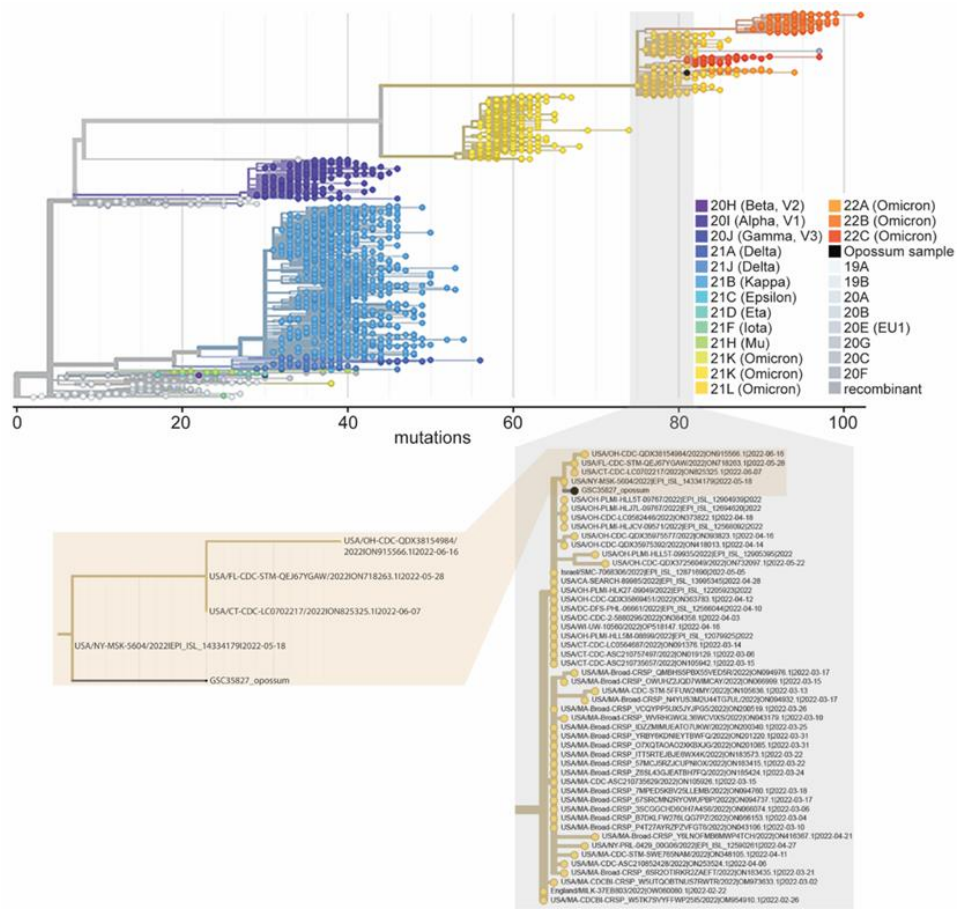

Figure 4. Whole Genome Sequencing of the Virginia opossum SARS-CoV-2 virus. Global phylogenetic tree using 2,001 sequences including the opossum SARS-CoV-2 whole genome sequence is shown clustering within the NextStrain clade 21L (BA.2; Omicron). Subtrees show the placement of the opossum SARS-CoV-2 sequence within the 20L cluster in more detail.

The $E^{471}V$ mutation is located in the receptor-binding motif (RBM, residues 437 to 508) within the receptor-binding domain (RBD, residues 319 to 541) of the S protein. The RBD is necessary for binding the viral S protein to ACE2 in both human and animal cells and is, in addition, therapeutically targeted by neutralizing monoclonal antibodies (21).

We performed a detailed computational investigation into the impact of the $E^{471}V$ and $G^{798}D$ mutations for the structure of the S protein using molecular modeling and molecular mechanics/generalized borne surface area (MM/GBSA) free energy calculations. The open conformation structure of the S protein trimer from the glycosylated BA.2 Omicron variant was used for residue variant mapping [PDB 7XO8; (22)]. Because the crystal structure shows the trimer bound to the human ACE2 (hACE2) receptor, it is possible to investigate the impact of mutations in the RBD on interactions between SARS-CoV-2 S protein and hACE2, as previously reported (23) (Fig. 4). Our free energy studies showed predicted free energy of binding between the $E^{471}V$-carrying mutation in S improved, compared to that of BA.2, for binding to hACE2 (-76.5 and -60.2 kcal/mol for E471V vs. BA.2, respectively). Residue 471 is predicted to be part of a flexible, hydrophobic loop that interacts with the N-terminal domain of ACE2 (Fig. 5). Several point mutations ($A^{475}V$, $S^{477}G$, $V^{483}A$, $F^{490}L$) within this loop region have experimentally shown to improve S protein – hACE2 binding affinity and increased resistance to neutralizing antibodies (24, 25). Our analysis using normalized Kyte-Doolittle hydropathy scores and surface maps show a more hydrophobic interaction surface at not just position 471, but also among flanking residues 469-474 (0.8) compared to BA.2 [-2.6; (26)].

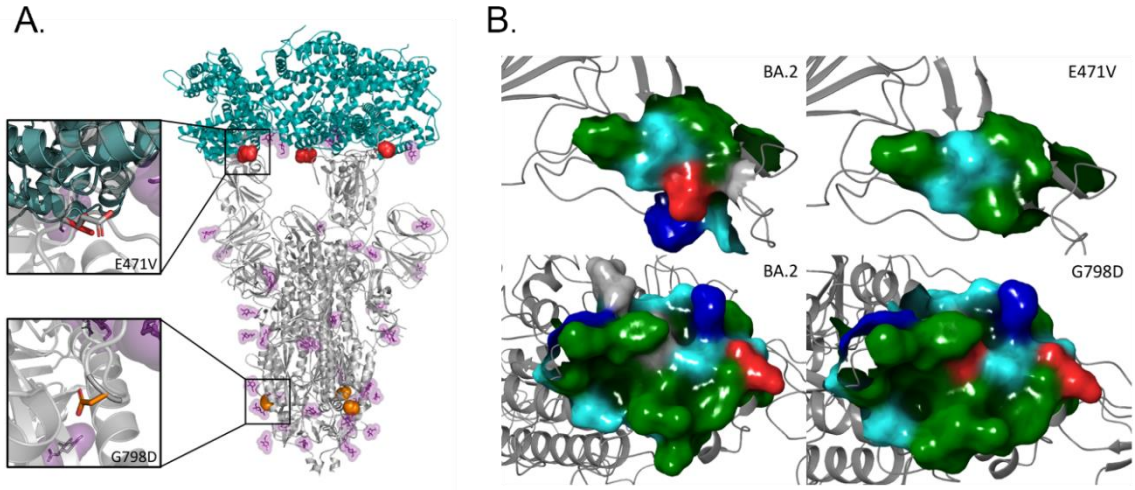

Figure 5. Molecular modeling of the unique S mutation of SARS-CoV-2 isolated from the Virginia opossum. (A) Representation of the structure of the BA.2 S protein (gray, PDB: 7XO8) in its open conformation bound to the human ACE2 (teal). Residues 471 (red) and 798 (orange) are shown as spheres. Glycans are displayed as sticks colored purple. Top inset: Overlay of $E^{471}V$ (red) and BA.2 (grey). Bottom inset: Overlay of $G^{798}D$ (orange) and BA.2 (grey). (B) Surface map of the BA.2 S protein (left) and the region surrounding $E^{471}V$ and $D^{798}G$ (right) residues.

Residue side chain properties are colored: green for hydrophobic, blue for positively charged, red for negatively charged, teal for polar uncharged, and gray for neutral.

We located a second missense mutation, $G^{798}D$, in the S2 subunit of the S protein (residues 686 to 1,273) and within the fusion peptide domain (residues 788 to 806) in close proximity to the N^{801} glycosylation site. Interestingly, D^{798} changed the probability of glycosylation at N^{801} (0.48) as compared to BA.2 [0.61, (27)] and could impact structural stability and membrane interaction (28) (Fig. 5 and Fig. S5).

Discussion

Our combined results suggest that a wide breadth of species may be exposed to SARS-CoV-2 in the wild. We detected positives in six species using RT-qPCR and neutralizing antibodies in an additional four species. We found support for a relationship between human presence and seroprevalence suggesting that areas with high human activity may serve as potential hotspots for cross-species transmission. Analysis of isolates collected from infected wildlife revealed novel mutations at the time of collection, some of which have subsequently been found circulating in other regions. Some of these mutations likely increase binding affinity to the hACE2 receptor or confer some antibody resistance compared to ancestral BA.2 lineages. Whether these mutations developed in humans not captured in surveillance at the time or in wildlife communities and were transmitted back to humans remains unknown but presents an important consideration for future variant surveillance.

SARS-CoV-2 PCR prevalence among wildlife was generally low and ranged from 1.6-20.0%. We found that 10.0% of opossums, a marsupial, were PCR positive (including equivocal detections), similar to PCR prevalence in white-tailed deer (10.0%) we tested. High seroprevalence (62%) and a single opossum with viral RNA at sufficient levels for WGS suggests this species may have high exposure to SARS-CoV-2 in natural settings. The SARS-CoV-2-positive opossum with two gene amplification was recaptured at the same site ~30 days later, and was positive for antibodies (51.1 % neutralization), supporting that the serology data reflect previous exposure to SARS-CoV-2.

We used a 50% neutralization cut-off value for our serological analyses of human use. We acknowledge that one sample collected prior to the arrival of SARS-CoV-2 had a percent neutralization value of 58% (a significantly higher percent neutralization than any of the other 66 samples; Fig. 2C, probability of false positive= 0.015). Given our post-SARS-CoV-2 seroprevalence estimates, the probability that we detected no positive samples in five species and one positive in one species prior to SARS-CoV-2 was very low (Table S5). A more conservative estimate such as raising the cutoff to 60%, would still yield positive samples from

five of the six species we sampled. However, a conclusively RT-qPCR positive opossum that was sampled one month later had a percent neutralization of only 51.1% (purple diamond, Fig. 2C), suggesting that more conservative estimates may miss previously exposed animals. Interestingly, samples below our 50% cutoff (classified as negative in our analyses) still tended to have higher percent neutralization post-SARS-CoV-2, possibly indicating waning immunity at the time of sampling.

Our seroprevalence results generally aligned with both experimental infection studies (e.g whether the species seroconverted) and predicted susceptibility based on ACE2 modeling (Table S8). Raccoons and skunks have been shown experimentally to be seroconvert following SARS-CoV-2 exposure (15, 29) and both had high seroprevalence in our study (64% and 67%, respectively). Deer mice have also been shown to be capable of viral shedding and producing neutralizing antibodies in the lab (13, 14, 29), are predicted to have high susceptibility, and had moderately high seroprevalence in this study (29%, Table S8). Eastern gray squirrels have not been evaluated through molecular modeling or experimental infections, but we had detections through both RT-qPCR (1.6%) and serology (71.4%). However, modeling of the functional receptor for SARS-CoV-2 (ACE2), with closely related species (red squirrels, (30)) predicted high susceptibility. Recent research has shown that the omicron (B.1.1.529) ACE2 binding affinity is greater in a number of wildlife species than in humans, including five marsupials (one of which is the Gray short-tailed opossum (*Monodelphis domestica*)), white-footed mouse, red fox, and two marmots, while deer mice and white-tailed deer were marginally below humans (31). This suggests that for species evaluated with earlier SARS-CoV-2 variants that did not seroconvert (fox squirrels) or shed virus (raccoons and squirrels), competence may now be higher with newer variants.

Many of the species in this study are considered human peridomestics and live in and around human settlements. Many of these species' range across large areas of North America and some have been introduced into Europe (gray squirrels and raccoons) and Asia (raccoons) and have close relatives across the globe. It is unknown whether a sylvatic cycle has been established in the species we evaluated, however, their close connection to human populations makes them important species for continued monitoring as they could be important for transmission to and from humans.

Our analyses revealed a relationship between human presence, urbanization and seroprevalence among sites. This suggests that wildlife in areas with more human activity likely have higher exposure to SARS-CoV-2, leading to more wildlife infections. Interestingly, the site with the highest seroprevalence was a forested recreational trail that receives high human visitation but is less developed. This suggests that recreational sites may be important points of contact between humans and wildlife and could be targeted for surveillance. Humans and wildlife

rarely come into direct contact, but numerous indirect links likely exist. Wastewater has been proposed as a potential source for indirect exposure to SARS-CoV-2 (32), however, in rural areas where septic tanks are a dominant form of wastewater management, this is unlikely to be the only source. Instead, other forms of human waste, like trash receptacles, may serve as important sources of indirect exposure for wildlife (15, 33). Urban wildlife are regularly exposed to human refuse and have developed positive associations with discarded food, which could serve as a bridge for transmission between humans, companion animals, and wild species (34-36). We regularly captured wildlife using traps baited with cat food and other common food items such as peanut butter, and thus may have attracted individuals with natural proclivities for human associated foods, thus inflating prevalence (e.g., these are the individuals who are already regularly coming into indirect contact with humans). More research is needed to understand transmission chains between humans, pets, and wildlife.

SARS-CoV-2 isolated from the opossum showed mutations in the RBM of the RBD of the S protein. The previously uncharacterized amino acid change is predicted to improve S-hACE2 binding compared to omicron BA.2, potentially providing a fitness advantage by either increasing the affinity of S for the ACE2 receptor or, alternatively, by evading the neutralizing activity of antibodies. These mutations were not observed in human samples at the time of isolation from the opossum and have only recently been identified in the Omicron sub-variant (BJ.1), with one mutation still remaining novel to the opossum sample. These results highlight the possible role of wildlife in contributing unique mutations that may be more transmissible to humans, as has been previously suggested with the emergence of the Omicron variant (5, 7).

Materials and Methods

Summary

Wildlife were sampled using nasopharyngeal and/or oropharyngeal swabs through active captures as well as through submissions to wildlife centers. At six sites we actively trapped wildlife using live-traps from May through July 2022. Sites were trapped 3-4 nights each depending on animal activity. We anesthetized and swabbed all animals and collected blood from a subset of individuals. Urbanization was calculated as the percent of impervious surface and adjusted based on the home range of each species captured. Human activity was estimated based on trail counters, visitation records or extrapolated from census data. We used generalized linear mixed models to evaluate relationships between seroprevalence and human presence and urbanization (See Supplemental Methods). This study was performed under Virginia Tech IACUC protocol #22-061.

Samples were RT-qPCR tested using our Emergency Use Authorized SARS-CoV-2 assay (37). Samples were reported conclusively positive when 2/3 SARS-CoV-2 genes (*N*, *E*, and *S*) and the housekeeping gene (Cytochrome C Oxidase Subunit 1; *Cox1;* Table S6) amplified

below the threshold established by corresponding standard curves (37). We did a full phylogenetic sequencing of SARS-CoV-2 from the opossum and conducted molecular modeling as indicated in Supplemental Methods. We used a plaque reduction neutralization test (PRNT) with a SARS-CoV-2 GNL-1205 stock. We categorized serum samples as positive if they had at least a 50% neutralization at a 1:20 dilution and negative if they had less than a 50% neutralization.

Study Sites

We collected nasopharyngeal or oropharyngeal samples from wildlife across 32 counties in Virginia, U.S.A. We collected samples from 3 wildlife rehabilitation centers in Boyce, Roanoke, and Waynesboro, VA. In addition, we actively captured wildlife from six sites that spanned a rural to urban gradient in Giles, Montgomery, Roanoke, and Wythe counties (Table S5, Fig. 1, see Supplemental Methods for site descriptions.).

Trapping and processing

We trapped each site for a 2-4 day session, and used 3 different sized live traps to capture animals: Tomahawk non-folding traps (Tomahawk Live Trap Co., Tomahawk, WI, U.S.A; 46 x 15 x 15cm, model 103.5), Tomahawk folding traps (66 x 23 x 23cm, model 205 or 81 x 25 x 31, model 207), and Sherman folding traps for smaller animals (Sherman Traps, Tallahassee, FL, U.S.A; 8 x 9 x 23cm, model LFG). We set and baited traps in the evening just before dark and checked them the following morning before 10:00 AM to ensure animals did not get overheated.

We processed all animals in the area where they were trapped. We anesthetized larger animals in either a bucket chamber (38) or in a 50L clear box chamber (58 x 38 x 56 cm, Fig. S5). We used a tec-4 funnel fill with a cage mount manifold vaporizer (Ohmeda, West Yorkshire, UK) connected to a portable medical oxygen cylinder (size E) with a built-in regulator (Walk-02-Bout+™, Airgas Healthcare, Radnor, PA). We used a 2 L/min oxygen mix to 3-4% isoflurane in the chambers. Smaller animals were placed in a small plastic canister and anesthetized with 0.5 – 1.2mL isoflurane (dosage depended on species and body size), placed onto a cotton ball held within a perforated canister to prevent direct contact with the animal. Once anesthetized, we removed animals from the chamber, and then masked animals (mice were only masked for collecting serum samples; Fig S6) with a dose of 2 L/min oxygen and 2-3% isoflurane.

We marked individuals with aluminum ear tags in each ear (National Band and Tag Company, model 1005-1 or 1005-3 depending on body size). We collected morphometric, sex and reproductive status from each animal. For RT-qPCR detections, we swabbed each individual with a polyester swab (25-800 1PD swab for larger mammals and 25-1000 1PD swab for smaller animals e.g. juveniles, skunks, squirrels, bats, shrews, and mice; Puritan Medical Products,

Guilford, ME, U.S.A). We used an oropharyngeal swab for animals that were too small for nasopharyngeal swabbing (mice, shrews, bats, etc.). All collection swabs were individually placed in tubes with solution (37) and kept in the shade until they were transported back to the laboratory following field work each day. Samples were then stored in the refrigerator at 3°C. Samples were processed within 5 days following field collection. We collected blood for antibody screening from the submandibular vein for mice and from the nail quick of one of the rear toenails for all other species. Blood was stored in microvette 500 z-gel tubes for later processing. All blood samples were put into a cooler immediately following field collection and placed in a refrigerator. All field personnel wore N95 masks and gloves to reduce the possibility of transmission between researchers and wildlife.

Wildlife Rehabilitation Sample Collection

Wildlife nasopharyngeal swabs were provided from 3 wildlife rehabilitation centers in Virginia. Swabs were placed in collection tubes with solution and kept in the refrigerator. They were returned and analyzed within 45 days of collection.

Sample testing

We carried out nucleic acid purification and amplification of SARS-CoV-2 using our Emergency Use Authorized SARS-CoV-2 assay as previously described with a few specific modifications [Federal Drug Administration, (37)]. Briefly, we processed swab-containing media shortly after collection and total RNA purified using 96-well spin columns, assessed for quality control, and subjected to synthesis and amplification using the Power SYBR™ Green RNA-to-CT™ 1-Step kit (Applied Biosystems). Our in-house test detects multiple targets including the nucleocapsid (*N*), envelope (*E*), and spike (*S*) genes of the SARS-CoV-2 virus, as well as the cytochrome c (Cox1) housekeeping gene for which species-specific primers were designed (Table S7). RT-qPCR reactions were performed in a CFX384 Touch Real-Time PCR Detection System (Bio-Rad), positive control using inactive SARS-CoV-2 virus (ATCC®), no template controls, and standard curves were included in each plate as previously described (37).

Serology data

Additional samples were obtained to compare seropositivity prior to the arrival of SARS-CoV-2 to those samples we collected. Samples were obtained from previous studies (Table S3). The samples were transferred to gold-top microtainer tubes (BD, Franklin Lakes, NJ, USA) and serum was separated via centrifugation at 5,000 x g for 10 minutes and transferred to 1.7 mL tubes. Serum samples were then heat inactivated at 55°C for 1 hour. Samples

were diluted 1:10 in RPMI-1640 with 10 mM HEPES and 2% FetalPure bovine serum (Genesee Scientific 25-525H). Diluted serum samples were mixed in a 1:1 v/v ratio with a solution containing 1300 plaque-forming units per mL (PFU/mL) of SARS-CoV-2 Delta virus strain USA-GNL-1205/2021 (a kind gift from the World Reference Center for Emerging Viruses and Arboviruses). Each sample was tested in triplicate. The mixture was then incubated at 37 °C for one hour, and then 50 µL of the virus-serum mixture was used to inoculate wells in a confluent 24-well plate of VeroE6 hACE2-TMPRSS2 cells and again incubated at 37 °C for one hour. After the one-hour adsorption period, we added 500 µL of overlay media to each well and incubated the plates at 37°C, as previously described (39). After 2 days, the plates were fixed with 10% formalin and stained with crystal violet. Based on previously published serosurveillance studies (40-43), we used the following testing criteria:

1. ≥ 90 % Neutralization at a 1:20 Dilution – Strong Positive
2. ≥ 50 % Neutralization at a 1:20 Dilution – Weak Positive
3. < 50 % Neutralization at 1:20 Dilution – Negative

We then ultimately decided to count any individual with at least a 50% neutralization as positive to analyze the effects of urbanization and human presence on SARS-CoV-2 exposure.

Urbanization and human presence variables

We obtained estimates of urban imperviousness from the National Land Cover Database 2019 (44, 45). We obtained estimates of population density from 2020 census at the 1km spatial scale (46). We created buffers of variable sizes based on species home range size to calculate the mean estimates of imperviousness and population density for each individual capture location (Table S7).

We obtained estimates of human presence at the 5 sites where we collected serology data (Table S5). New River Trails State Park and Roanoke Parks and Recreation provided monthly human visitation estimates between March and August 2022. Mountain Lake Biological Research Station provided us an estimate for how many people were using the facilities at the station between March and August 2022; they averaged about 50 people at the station per month and we multiplied it by 7 (1 week) to represent that each person may have stayed ~7 days. Brush Mountain recreational area was closed to the public from March through August 2022 so we assumed approximately 10 people used the area per month. For the town of Blacksburg, we used population estimates from the 2020 census (TIGER/Line, U.S. Census Bureau, 2020 Blocks). We created a minimum convex polygon (mcp) in the adehabitatHR package (47) in program R v 4.1.1 (48) around the different trapping locations. We used ArcGIS Pro (ArcGIS Pro 2.9.0, Esri, Redlands, CA, USA) to calculate the population within each mcp area. We used the intersect tool field calculator, and summary statistics to calculate the population for each census block by

multiplying the percent of the block within the mcp by the population count. We then summed the population within the mcp to estimate the total population. We multiplied the population count by 30 to estimate the number of people per month using that area.

Similarly, we used resident population estimates from the 2020 census. We used the same mcp's for each site as described above. We then added a 1km buffer area around each census assuming both animals and residents move in and out of the trapping mcp area. As described above, we calculated the percentage that each census block fell within the buffered mcp area and summed the counts to provide an estimate of the resident population at each site.

Whole genome sequencing and Sanger amplification

To amplify the entire SARS-CoV-2 genome, positive samples were reverse transcribed and amplified using SuperScript IV Reverse Transcriptase (Thermofisher) and ARTIC nCoV-2019 Amplicon Panel V4.1 primers (Integrated DNA technologies). Purified PCR products were barcoded using the plexWell™ 384 Library Preparation Kit (seqWell, MA) and the pooled library sequenced using a MiSeq System (Illumina, CA) following manufacturer's instructions. SARS-CoV-2 sequencing analysis was accomplished using an established pipeline and optimized workflow for validation that combines tools to assess quality, sequence alignment, variation calling, and variant assignment. We processed lineage assignments using Pangolin software suite (https://cov-lineages.org/) (49). Whole genome sequences were deposited in the GISAID database (https://www.gisaid.org/) and NCBI (https://ncbi.nlm.nih.gov) SARS-CoV-2 sequence repositories.

Phylogenetic analysis

A FASTA file containing the opossum SARS-CoV-2 whole genome sequence was uploaded in Ultrafast Sample placement on Exiting tRee [UShER; https://genome.ucsc.edu/cgi-bin/hgPhyloPlace, (50, 51)] for global phylogenetic tree analysis using 12,397,869 SARS-CoV-2 genomes obtained from GISAID, GenBank, COG-UK and CNCB that were available as of 2022-10-03. The resulting global tree and subtree were visualized using NextStrain's interactive display [https://nextstrain.org/, (52)] and 2001 and 50 sequences, respectively.

Molecular modeling

We carried out computational studies of the structure of the glycosylated Omicron BA.2 variant bound to the human ACE2 receptor [Protein Data Bank 7XO8;

(22)]. We incorporated point mutations in BA.2 using PyMOL (The PyMOL Molecular Graphics System v. 2.4.0, Schrödinger, LLC) to generate a new structure containing both E471V and G798D mutations. We then performed energy minimization using Schrödinger-Maestro (v. 2020.4) and OPLS3e force field (53, 54). We used Schrödinger Bioluminate to carry out molecular mechanics/generalized borne surface area (MM/GBSA) energy calculations (55, 56) as well as surface mapping [v. 2020.4; (26)]. Glycosylation propensity was calculated using the NetNGlyc 1.0 server (57).

Genomic data

Human (13,221) and wildlife (333) clinical samples were analyzed for the presence of SARS-CoV-2 by RT-qPCR as described in the Summary section. We considered samples conclusively positive when 2 of 3 SARS-CoV-2 genes (*N*, *E*, and *S*) and the housekeeping gene (*RPP30* for humans and *COX1* for wildlife) amplified below the threshold established by corresponding standard curves (37). We performed whole genome and amplicon sequencing for conclusively positive samples (Fig. 1A). We limited the description of variants in the human population to the window at which wild sample collection took place (May 1, 2022 to September 8, 2022).

The analysis of human clinical specimens identified 4, 123, 8, 350, 162, 586 as positive, negative, inconclusive, or invalid (no housekeeping gene detected), respectively (Fig. S3A). All positive samples with Cq values <33 were sequenced and have a variant assignment. A few samples failed sequencing or were not assigned due to their quality/quantity and low sequence depth. As shown in Fig. S3B, various SARS-CoV-2 lineages expanded the window of our study with BA.1 (0.17%), BA.2 (15.85%), BA.2.12.1 (25.80%), BA.4 (14.83%), BA.5 (37.91%), BE (1.57%), BF (1.45%), BG.2 (0.05%), AY.103 (0.02%), no assigned (N/A, 2.24%) being the most prevalent among humans in the region.

Statistical Analyses

We used the sf (58) and exactextractr (59) packages in program R to calculate the mean of the urbanization variables within each of our trap buffers. We calculated prevalence 95% confidence intervals using the “PropCIs” package (60) and the Agresti-Coull method due to small sample sizes. We used the glmmTMB package (61) in program R to analyze univariate generalized linear mixed models to assess whether seroprevalence rates were impacted by the following covariates: urbanization (imperviousness), human presence, and resident population and included species as a random effect. All P-values presented represent a 2-tailed test.

Acknowledgments

We thank the following for land access: J Eustis and New River Land Trust; B Brodie, J Jones and Mountain Lake Biological Research Station; R Powers, K Slusher, A McGee and Roanoke Parks and Recreation; V Malzone, G Gorecki, S Sweeney, J Elliott, and Virginia State Parks; G O'Malley, A Lewis, H Wander, K Malewicz, V Corbin, R Cohen, S Whitehead and family, N Laggan, A Grimaudo, and G Blanvillain. We thank the following for help with study design and collection: M Fisher, J Ivan, K Bentler, S Yamada, C Cereghino, K Pierce and the Wildlife Center of Virginia, J Riley and the Blue Ridge Wildlife Center, and H Olsen-Hodges and the Southwest Virginia Wildlife Center. Additionally, we thank G. Eastwood and A. M. Kilpatrick, and NEON Biorepository for sharing serum samples with us. This project was supported by funds NSF DEB-1911853 to K.E.L. and J.R.H., the Virginia Tech FBRI to C.V.F., and a One Health award from VCOM to J.W.

Data Availability

All study data are included in the article and supporting information. Sequence data from SARS-CoV-2 viruses from Virginia opossum sequenced in this study are available in the GISAID database (https://www.gisaid.org/) and NCBI (https://ncbi.nlm.nih.gov) SARS-CoV-2 sequence repositories.

References

1. World Health Organization (2020) WHO COVID-19 Dashboard. (Geneva).
2. M. Drozdz *et al.*, Current State of Knowledge about Role of Pets in Zoonotic Transmission of SARS-CoV-2. *Viruses-Basel* **13**, 1149 (2021).
3. M. Fritz *et al.*, High prevalence of SARS-CoV-2 antibodies in pets from COVID-19+ households. *One Health* **11**, 100192 (2020).
4. H. L. Murphy, H. Ly, Understanding the prevalence of SARS-CoV-2 (COVID-19) exposure in companion, captive, wild, and farmed animals. *Virulence* **12**, 2777-2786 (2021).
5. V. L. Hale *et al.*, SARS-CoV-2 infection in free-ranging white-tailed deer. *Nature* **602**, 481-486 (2022).
6. J. C. Chandler *et al.*, SARS-CoV-2 exposure in wild white-tailed deer (*Odocoileus virginianus*). *P Natl Acad Sci USA* **118**, e2114828118 (2021).
7. S. V. Kuchipudi *et al.*, Multiple spillovers from humans and onward transmission of SARS-CoV-2 in white-tailed deer. *P Natl Acad Sci USA* **119**, e2121644119 (2022).
8. B. Davoust *et al.*, Evidence of antibodies against SARS-CoV-2 in wild mustelids from Brittany (France). *Transboundary and Emerging Diseases* **69** (2022).
9. J. Aguiló-Gisbert *et al.*, First description of SARS-CoV-2 infection in two feral American mink (*Neovison vison*) caught in the wild. *Animals* **11**, 1422 (2021).
10. M. Padilla-Blanco *et al.*, The finding of the severe acute respiratory syndrome coronavirus (SARS-CoV-2) in a Wild Eurasian River Otter (*Lutra lutra)* highlights the need for viral surveillance in wild mustelids. *Front Vet Sci* **9** (2022).

11. F. Martínez-Hernández *et al.*, Assessing the SARS-CoV-2 threat to wildlife: Potential risk to a broad range of mammals. *Perspectives in ecology and conservation* **18**, 223-234 (2020).
12. D. A. Meekins, N. N. Gaudreault, J. A. Richt, Natural and Experimental SARS-CoV-2 Infection in Domestic and Wild Animals. *Viruses-Basel* **13**, 1993 (2021).
13. B. D. Griffin *et al.*, SARS-CoV-2 infection and transmission in the North American deer mouse. *Nature Communications* **12**, 10 (2021).
14. A. Fagre *et al.*, SARS-CoV-2 infection, neuropathogenesis and transmission among deer mice: Implications for spillback to New World rodents. *PLoS Pathog.* **17**, 23 (2021).
15. R. Francisco *et al.*, Experimental Susceptibility of North American Raccoons (Procyon lotor) and Striped Skunks (Mephitis mephitis) to SARS-CoV-2. *Front Vet Sci* **8**, 10 (2022).
16. L. C. Caserta *et al.*, White-tailed deer (Odocoileus virginianus) may serve as a wildlife reservoir for nearly extinct SARS-CoV-2 variants of concern. *P Natl Acad Sci USA* **120**, 12 (2023).
17. L. G. Thorne *et al.*, Evolution of enhanced innate immune evasion by SARS-CoV-2 (vol 602, pg 487, 2022). *Nature* **604**, E14-E14 (2022).
18. B. Pickering *et al.*, Divergent SARS-CoV-2 variant emerges in white-tailed deer with deer-to-human transmission. *Nat. Microbiol* 10.1038/s41564-022-01268-9, 23.
19. C. C. S. Tan *et al.*, Transmission of SARS-CoV-2 from humans to animals and potential host adaptation. *Nature Communications* **13**, 13 (2022).
20. S. Alizon, M. T. Sofonea, SARS-CoV-2 virulence evolution: Avirulence theory, immunity and trade-offs. *J Evolution Biol* **34**, 1867-1877 (2021).
21. P. C. Taylor *et al.*, Neutralizing monoclonal antibodies for treatment of COVID-19. *Nat. Rev. Immunol.* **21**, 382-393 (2021).
22. Z. Xu *et al.*, Integrated strategy of RNA-sequencing and network pharmacology for exploring the protective mechanism of Shen-Shi-Jiang-Zhuo formula in rat with non-alcoholic fatty liver disease. *Pharm Biol* **60**, 1819-1838 (2022).
23. Y. F. Kang *et al.*, Rapid Development of SARS-CoV-2 Spike Protein Receptor-Binding Domain Self-Assembled Nanoparticle Vaccine Candidates. *Acs Nano* **15**, 2738-2752 (2021).
24. V. Singh *et al.*, Stroke increases the expression of ACE2, the SARS-CoV-2 binding receptor, in murine lungs. *Brain Behav Immun* **94**, 458-462 (2021).
25. H. D. Li *et al.*, Greener liquid-phase synthesis and the ACE inhibitory structure-activity relationship of an anti-SARS octapeptide. *Org Biomol Chem* **18**, 8433-8442 (2020).
26. H. Beard, A. Cholleti, D. Pearlman, W. Sherman, K. A. Loving, Applying Physics-Based Scoring to Calculate Free Energies of Binding for Single Amino Acid Mutations in Protein-Protein Complexes. *Plos One* **8**, e82849 (2013).
27. M. Huang *et al.*, Atlas of currently available human neutralizing antibodies against SARS-CoV-2 and escape by Omicron sub-variants BA.1/BA.1.1/BA.2/BA.3. *Immunity* **55**, 1501-1514 (2022).
28. A. Shajahan, L. E. Pepi, D. S. Rouhani, C. Heiss, P. Azadi, Glycosylation of SARS-CoV-2: structural and functional insights. *Analytical and Bioanalytical Chemistry* **413**, 7179-7193 (2021).
29. A. M. Bosco-Lauth *et al.*, Peridomestic mammal susceptibility to severe acute respiratory syndrome coronavirus 2 infection. *Emerg Infect Dis* **27**, 2073 (2021).

30. S. Pach *et al.*, ACE2-Variants Indicate Potential SARS-CoV-2-Susceptibility in Animals: A Molecular Dynamics Study. *Molecular Informatics* **40** (2021).
31. A. Samanta, S. S. M. Alam, S. Ali, M. Hoque, Evaluating the transmission feasibility of SARS-CoV-2 Omicron (B.1.1.529) variant to 143 mammalian hosts: insights from S protein RBD and host ACE2 interaction studies. *Functional & Integrative Genomics* **23** (2023).
32. A. B. Franklin, S. N. Bevins, Spillover of SARS-CoV-2 into novel wild hosts in North America: A con- ceptual model for perpetuation of the pathogen. *Sci. Total Environ.* **733**, 139358 (2020).
33. J. Han *et al.*, Municipal solid waste, an overlooked route of transmission for the severe acute respiratory syndrome coronavirus 2: a review. *Environ. Chem. Lett.* 10.1007/s10311-022-01512-y, 1-15 (2022).
34. M. A. Aberle, K. E. Langwig, J. S. Adelman, D. M. Hawley, Effects of bird feeder density on the foraging behaviors of a backyard songbird (the House Finch, Haemorhous mexicanus) subject to seasonal disease outbreaks. *Canadian Journal of Zoology* **98**, 611-621 (2020).
35. D. J. Civitello, B. E. Allman, C. Morozumi, J. R. Rohr, Assessing the direct and indirect effects of food provisioning and nutrient enrichment on wildlife infectious disease dynamics. *Philos T R Soc B* **373** (2018).
36. T. Longcore, C. Rich, L. M. Sullivan, Critical Assessment of Claims Regarding Management of Feral Cats by Trap-Neuter-Return. *Conserv Biol* **23**, 887-894 (2009).
37. A. Ceci *et al.*, Development and implementation of a scalable and versatile test for COVID-19 diagnostics in rural communities. *Nature Communications* **12**, 1-14 (2021).
38. K. T. Bentler, D. N. Gossett, J. J. Root, A novel isoflurane anesthesia induction system for raccoons. *Wildlife Society Bulletin* **36**, 807-812 (2012).
39. J. L. Liu *et al.*, Stabilization of a Broadly Neutralizing Anti-Chikungunya Virus Single Domain Antibody. *Front Med (Lausanne)* **8**, 626028 (2021).
40. A. M. Bosco-Lauth *et al.*, Experimental infection of domestic dogs and cats with SARS-CoV-2: Pathogenesis, transmission, and response to reexposure in cats. *Proceedings of the National Academy of Sciences* **117**, 26382-26388 (2020).
41. A. M. Bosco-Lauth *et al.*, Susceptibility of livestock to SARS-CoV-2 infection. *Emerging Microbes & Infections* **10**, 2199-2201 (2021).
42. S. A. Shriner *et al.*, SARS-CoV-2 Exposure in Escaped Mink, Utah, USA. *Emerg Infect Dis* **27**, 988-990 (2021).
43. P. M. Palermo, J. Orbegozo, D. M. Watts, J. C. Morrill, SARS-CoV-2 Neutralizing Antibodies in White-Tailed Deer from Texas. *Vector Borne Zoonotic Dis* **22**, 62-64 (2022).
44. J. Dewitz, U.S. Geological Survey National Land Cover Database (NLCD) 2019 Products. Deposited 2021.
45. J. Wickham, S. V. Stehman, D. G. Sorenson, L. Gass, J. A. Dewitz, Thematic accuracy assessment of the NLCD 2016 land cover for the conterminous United States. *Remote Sens Environ* **257**, 112357 (2021).
46. Center for International Earth Science Information Network (CIESIN), Gridded Population of the World, Version 4 (GPWv4): Population Density, Revision 11. NASA Socioeconomic Data and Applications Center (SEDAC). https://doi.org/10.7927/H49C6VHW.

47. C. Calenge, The package "adehabitat" for the R software: A tool for the analysis of space and habitat use by animals. *Ecol Model* **197**, 516-519 (2006).
48. R Core Team (2021) R: A Language and Environment for Statistical Computing. (R Foundation for Statistical Computing, Vienna, Austria).
49. A. O'Toole *et al.*, Assignment of epidemiological lineages in an emerging pandemic using the pangolin tool. *Virus Evol* **7** (2021).
50. P. Sagulenko, V. Puller, R. A. Neher, TreeTime: Maximum-likelihood phylodynamic analysis. *Virus Evol* **4** (2018).
51. Y. Turakhia *et al.*, Ultrafast Sample placement on Existing tRees (UShER) enables real-time phylogenetics for the SARS-CoV-2 pandemic. *Nat Genet* **53**, 809-816 (2021).
52. J. Hadfield *et al.*, Nextstrain: real-time tracking of pathogen evolution. *Bioinformatics* **34**, 4121-4123 (2018).
53. E. Harder *et al.*, OPLS3: A Force Field Providing Broad Coverage of Drug-like Small Molecules and Proteins. *J Chem Theory Comput* **12**, 281-296 (2016).
54. D. Shivakumar *et al.*, Prediction of Absolute Solvation Free Energies using Molecular Dynamics Free Energy Perturbation and the OPLS Force Field. *J Chem Theory Comput* **6**, 1509-1519 (2010).
55. M. P. Jacobson, R. A. Friesner, Z. X. Xiang, B. Honig, On the role of the crystal environment in determining protein side-chain conformations. *J Mol Biol* **320**, 597-608 (2002).
56. M. P. Jacobson *et al.*, A hierarchical approach to all-atom protein loop prediction. *Proteins* **55**, 351-367 (2004).
57. K. Julenius, NetCGlyc 1.0: prediction of mammalian C-mannosylation sites. *Glycobiology* **17**, 868-876 (2007).
58. E. Pebesma, Simple Features for R: Standardized Support for Spatial Vector Data. *R J* **10**, 439-446 (2018).
59. D. Baston (2020) exactextractr: Fast extraction from raster datasets using polygons. in *R package version 0.5. 0*.
60. R. Scherer (2018) PropCIs: Various Confidence Interval Methods for Proportions.
61. M. E. Brooks *et al.*, glmmTMB balances speed and flexibility among packages for zero-inflated generalized linear mixed modeling. *The R journal* **9**, 378-400 (2017).
62. National Ecological Observatory Network, NEON Biorepository Mammal Collection (Blood Samples). *Occurrence dataset https://doi.org/10.15468/vqy6fj accessed via the NEON Biorepository Data Portal, https://biorepo.neonscience.org/ on 2023-05-08.* (2023).
63. A. Gomez *et al.*, Land use and West Nile Virus seroprevalence in wild mammals. *Emerg Infect Dis* **14**, 962-965 (2008).
64. I. R. Fischhoff, A. A. Castellanos, J. P. Rodrigues, A. Varsani, B. A. Han, Predicting the zoonotic capacity of mammals to transmit SARS-CoV-2. *Proceedings of the Royal Society B* **288**, 20211651 (2021).
65. L. L. Wu *et al.*, Broad host range of SARS-CoV-2 and the molecular basis for SARS-CoV-2 binding to cat ACE2. *Cell Discov.* **6**, 12 (2020).